NUV Silicon Photomultipliers with high detection efficiency and reduced delayed correlated-noise

Fabio Acerbi, *Member, IEEE,* Alessandro Ferri, Gaetano Zappala, Giovanni Paternoster, Antonino Picciotto, Alberto Gola, *Member, IEEE,* Nicola Zorzi, Claudio Piemonte, *Member, IEEE*

***Abstract*— In this paper, we present the characteristics and performances of new silicon photomultipliers (SiPMs), produced at FBK, for the near-ultraviolet (NUV) light detection, with reduced after-pulsing and delayed optical cross-talk. To study these components of the correlated noise, we manufactured SiPMs on silicon wafers featuring different substrate minority-carrier lifetime. This parameter proved to be crucial in determining the amount of delayed optical cross-talk and after-pulsing caused by photo-generated carriers diffusing from the substrate to the cell active-region. With a very low substrate lifetime we were able to minimize this correlated noise component to few percent at room temperature. Besides reducing the excess noise factor, the lower delayed correlated noise allows biasing the SiPM at higher voltages, reaching higher values of photon detection efficiency.**

***Index Terms*—, After-pulsing, carrier lifetime, optical cross-talk, photon number resolution, silicon photomultiplier, SiPM.**

I. Introduction

SILICON photomultiplier (SiPM) has obtained a growing attention as an alternative to the traditional photomultiplier tube in the detection of low photon fluxes thanks to a number of advantages typical of solid state detector, such as compactness, ruggedness, ease of use, low operational voltage and insensitivity to magnetic fields [1]. SiPM can be successfully used for fast detection of scintillation light, e.g., in nuclear medicine and high-energy physics. For example, it allows important advancements in positron emission tomography (PET) where its small size and insensitivity to magnetic fields allow a compact packing and the combination with magnetic resonance imaging [2]. Further, the good time resolution permits time-of-flight (TOF) PET, which improves image quality [3][4][5].

In a large number of applications exploiting scintillators, the light to be detected is in the blue or near-ultraviolet (NUV) region. For example, in positron emission tomography (PET), SiPMs are usually coupled to scintillators like LYSO:Ce (peak emission at 420 nm) or LaBr:Ce (at 380 nm) [6]. Thus, for efficient detection of this light, a p-on-n configuration with detection efficiency peaked around 400 nm has to be used [7][8][9].

The first of these devices produced at FBK (called NUV-SiPM, with a p-on-n junction type) proved good performances, with a primary dark count rate in the order of 100-200 kcps/mm^2 (kilo counts-per-second per 1-mm^2) [7]. However, they suffered from the delayed correlated noise (i.e., delayed crosstalk and afterpulsing), which is higher than in the corresponding n-on-p counterpart for green light detection ("RGB-SiPM" [10]). This limited their maximum operating bias, thus the maximum achievable photo-detection efficiency (PDE) and best timing resolution.

In this paper, we present the characteristics and performance of new NUV-SiPMs manufactured on different type of silicon substrates, with the aim to reduce the delayed correlated noise. We will show how the semiconductor lifetime affects the main SiPM parameters, e.g., the afterpulsing and crosstalk probabilities, the maximum operating voltage and, as a consequence, the photon detection efficiency.

II. Device structure

The devices presented in this paper are called NUV-SiPM, because of the peak photon detection efficiency in the near-UV region. Near-UV photons are absorbed very close to the surface in silicon (e.g., absorption length is ~ 34 nm at λ=380 nm), thus the junction depth, i.e. nearly the upper border of depleted active region, must be very shallow to enhance quantum efficiency. Moreover, in a Geiger-mode device like a SiPM, also the avalanche triggering probability has to be considered [11][12]. A p+/n junction type is required to trigger the avalanche (by photon absorbed superficially) mainly with electrons: the ionization coefficient for electrons is higher than for holes at a given bias voltage, thus the triggering probability is higher.

The layout of the new NUV-SiPMs (schematized in Fig. 1) has narrower border between cells: the cell size is 40 µm (i.e., the pitch between cells) and the fill factor (FF) is about 60%.

This work was supported in part by the European Community Seventh Framework Programme (EU FP7) Project SUB nanosecond Leverage In PET/MR ImAging (SUBLIMA) under Grant 241711.

Fabio Acerbi, Alessandro Ferri, Gaetano Zappala, Giovanni Paternoster, Antonino Picciotto, Alberto Gola, Nicola Zorzi and Claudio Piemonte are with Fondazione Bruno Kessler (FBK), Center for Materials and Microsystems (CMM), via Sommarive, 18, I-38123 Trento, Italy (email: acerbi@fbk.eu; aleferri@fbk.eu; zappala@fbk.eu; paternoster@fbk.eu; picciotto@fbk.eu; gola@fbk.eu; zorzi@fbk.eu; piemonte@fbk.eu). Gaetano Zappala is also with University of Trento, Department of Physics, via Sommarive 14, Trento, Italy (email: zappala@fbk.eu)

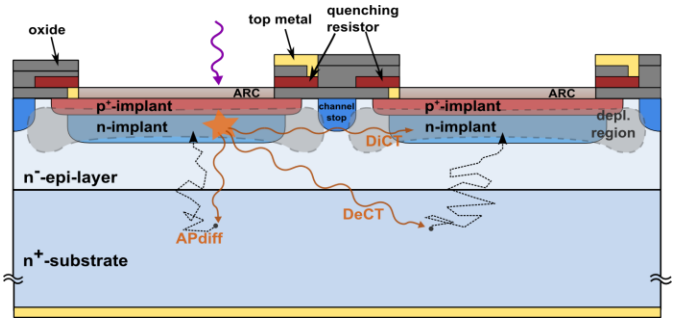

Fig. 1 Structure of the NUV-SiPM with the main correlated noise sources (afterpulsing, not represented, direct crosstalk, DiCT, delayd crosstalk, DeCT, and afterpulsing from diffused carriers, APdiff).

It is higher than in the previous version, where it was ~ 42% for the 50-µm cell [7]. The higher fill-factor is useful to improve the PDE, but the narrower border typically increases the crosstalk between cells, both the direct and the delayed crosstalk component (described in the next session). Therefore, it is generally not straightforward to both increase the PDE and reduce the correlated noise.

III. Correlated Noise Sources

The main sources of correlated noise in SiPMs are represented in Fig. 1: i) *afterpulsing*, which can be either due to trapped-and-released carriers in the active region or due to photo-generated carriers diffusing from the substrate (AP_{diff}); ii) *optical cross-talk*, which can be either due to direct absorption of secondary photons in the neighbor-cells active region (DiCT) or due to photo-generated carriers diffusing from the substrate to neighbor cell. The latter is originated by physical processes similar to APdiff but produces pulses in neighbor cells (thus crosstalk) delayed in time with respect to the first avalanche that generated the correlated event, thus it is called delayed crosstalk (DeCT), as in [7][13]. It can also be referred as diffused crosstalk, CTdiff, as in [14] .

The DeCT and AP_{diff} depend on the properties of the substrate, for example the "quality" (in terms of defects concentration): the lower the defect concentration the higher is the lifetime of photo-generated carriers and the higher the probability of delayed crosstalk. Conversely, DiCT depends only on cell layout and thickness of active depleted region. Afterpulsing due to trapped carriers in the active region depends mainly on cell gain and defect concentration in the epitaxial layer.

As a first approximation, the probability of a delayed cross-talk event (P_{DeCT}), once the secondary-photon generated by an avalanche produced an electron-hole pair in the substrate, under a neighbor active cell, exponentially decrease with the ratio between the distance (from the absorption point and the active region) and the minority carrier diffusion length. This approximation is partially justified since the cell side is much larger than the epi-layer thickness and diffusion length. The AP_{diff} probability also has a similar dependence, but it also depends on the cell recharge time: diffused carriers cannot trigger avalanches in a cell that is not yet recharged enough.

To reduce the DeCT and AP_{diff}, some structural solutions could be employed, e.g., deep trenches between cells to prevent photons to travel underneath neighboring cells, and a p-type substrate. The latter (in a p-on-n structure, like in Fig. 1) creates a second junction between epitaxial layer and substrate, preventing carriers generated in the substrate to diffuse into the epitaxial layer (and the depleted region) [15][16], but this would require more complex metal connection and biasing scheme.

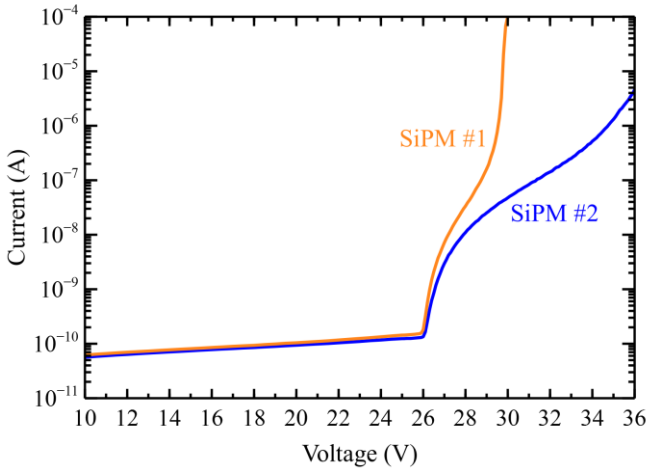

Fig. 2 Reverse I-V curve of 1x1 mm^2 SiPMs with substrate type 1 and type 2.

To reduce the delayed correlated noise, we followed a different approach manufacturing the devices on a different kind of substrate, called substrate #2, with reduced carrier lifetime (more than one order of magnitude lower) than in the previous one, called substrate #1. To have a direct performance comparison, we fabricated devices with the same layout and epitaxial layer. We identify these devices respectively as SiPM #1 (with substrate #1) and SiPM #2 (substrate #2).

IV. Experimental Results

In the following paragraphs, we present a set of measurements that gives a complete picture of the devices performance, in dark conditions, and with continuous and pulsed light, highlighting the effect of the new low-lifetime substrate. Functional measurements were performed on 1x1 mm^2 SiPMs, inside a thermostatic chamber with a front-end based on an AD8000 amplifier in trans-impedance configuration.

A. *I-V curve*

Fig. 2 shows the I-V curves of SiPM #1 and SiPM #2. It can be noted that the breakdown voltage is the same since it does not depend on the substrate characteristics. The post-breakdown current, which is determined by primary and correlated avalanches, is very different in the two devices. In particular, the divergence, due to the high correlated event probability, is more relevant in SiPM #1 limiting the operating excess-bias range to only ~3 V. Conversely, the new SiPM #2 shows a reduced divergence of the I-V curve and it can operate at excess bias higher than ~6 V.

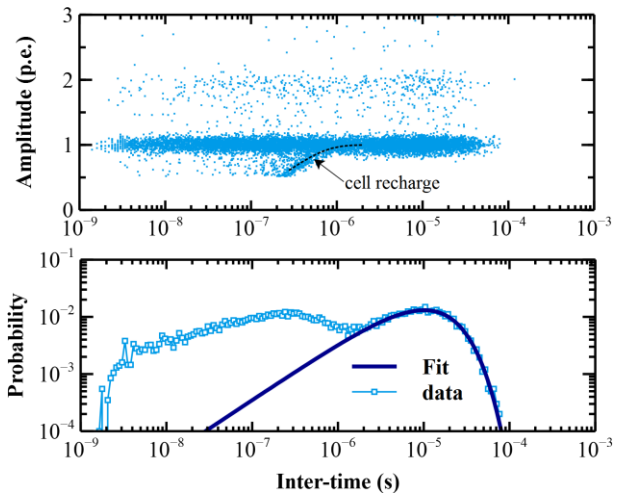

Fig. 3 Scatter plot of avalanche pulse amplitude (expressed in number of photo-electron, p.e.) vs. inter-time, after previous avalanche (top) (10000 events collected) and event probability vs. inter-times (bottom), for SiPM #1, at 20°C and 2.5V of excess bias.

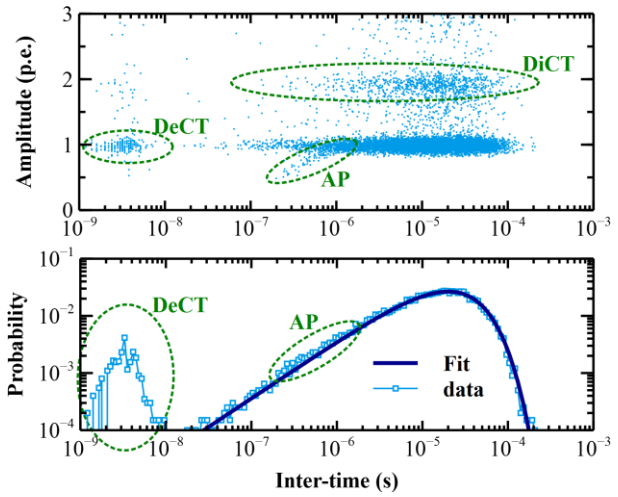

Fig. 4 Scatter plot of avalanche pulse amplitude vs. time after previous avalanche (top) and event probability vs. inter-times histogram (bottom), for SiPM #2, at 2.5V, 20°C.

B. Noise characterization

We measured the noise properties of the SiPMs in dark condition following the procedure described in [13]: we acquire ~ 1-ms long SiPM signal waveforms and, after filtering and pulse identification, we plot the pulse amplitude vs. the inter-time (i.e., the time between the pulse and its previous one). This allows discriminating the different components of the device noise.

Two examples of this measurement, related to SiPM #1 and #2 respectively, at 20°C and 2.5 V of excess bias, are shown in the upper plots of Fig. 3 and Fig. 4. The different noise contributions are highlighted only in Fig. 4 where they are better distinguishable. The events with unitary amplitude and inter-times > 10 ns are primary events, whereas the events with double or triple amplitudes are due to DiCT (calculated from the 2 p.e. on 1 p.e. probability ratio). Pulses occurring within the same pixel at short time-distance have an amplitude following the cell recovery curve 1-exp(-t/τ), as shown in Fig.

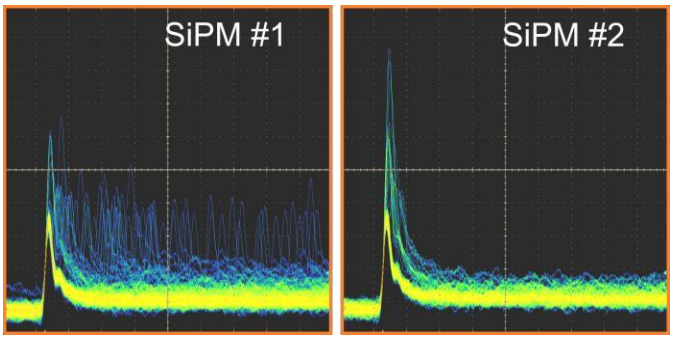

Fig. 5 Superposition of oscilloscope traces (10mV/div, 10ns/div), showing the avalanche pulse distribution, of 1x1 mm^2 NUV-SiPM with substrate #1 (left) and with substrate #2 (right), acquired at 2.5 V of excess bias, at -20 °C.

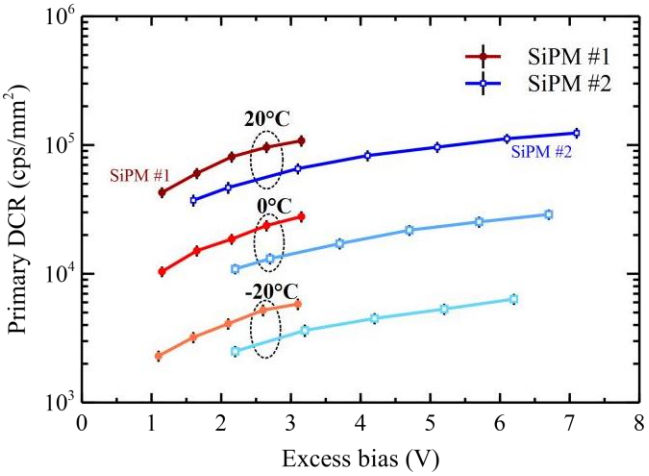

Fig. 6 Primary dark count rate (per square millimeter) of SiPM with substrate #1 and #2, as a function of excess bias, at different temperatures.

3, where τ~300ns; these are due to afterpulsing, either from trap release or hole diffusion from the substrate.

The lower plots of the same Figures represent the probability of an event to happen at a certain inter-time. They are obtained from their respective scatter plots dividing the number of counts in a time-bin by the total number of events and not considering their amplitude. Pulses occurring after 10 μs are all primary dark counts; the primary dark-count-rate (DCR) is extrapolated by fitting the late part of the spectrum with a Poisson distribution (shown by the continuous line). This fit, in a linear scale has an exponential shape, but in a log-log plot, with logarithmic bin-size, has the profile shown in the figure. Most of the pulses occurring at time difference <1 μs are not dark counts, but they are originated either by delayed crosstalk or afterpulsing. Thanks to the good separation between the two contributions, in SiPM #2, we can calculate the amount of DeCT as the integral of difference between the measured data and the Poisson's fit from 0 up to 10-20 ns. The AP can be evaluated with the same procedure but integrating from 100 ns to about 10 μs.

It can be seen that the amount of non-primary events is much higher in SiPM with substrate #1, compared to substrate #2, indicating a more relevant correlated noise. The delayed crosstalk events (approximately 43% of the total) happen from few nanosecond to few microseconds after primary avalanche

pulses, whereas afterpulsing events (approximately 6%) start at about 200 ns (for both the SiPMs, since they have the same quenching resistor). In SiPM #2 there are only few after-pulses (~ 0.5%) and the delayed crosstalk runs out in only ~ 10 ns (being ~ 3.5%). It should be noted that, since the substrate carrier lifetime (< 10 ns) is much lower than the recharge time of the cells (~ 200 ns), AP_{diff} is practically negligible and the afterpulsing is only due to trapped and released carriers in the active region (in the order of 0.5%).

From the scatter plots it also appears that the number of events at amplitudes larger than 1 has increased from type #1 to type #2. This means that the direct cross talk probability has unexpectedly increased. We found it to be twice as large. The reason for this increment is still under investigation.

Considering the parameters of the silicon materials provided by the substrate manufacturer, we estimated a hole lifetime of about 400ns for substrate #1, giving a diffusion length of about 6 µm within the silicon, whereas it is reduced to ~2 ns for substrate #2, giving a diffusion length of only 400 nm. This big difference is in agreement with the "extinction times" of delayed correlated noise seen in the histograms: if we consider 5 times the lifetime (to have a complete recombination of carriers), we have ~2 µs for SiPM #1 and ~10 ns for SiPM #2.

All these considerations are qualitatively visible also from the oscilloscope traces of the two SiPMs, as shown in Fig. 5 (they are triggered on half of 1-photon amplitude). The large number of delayed pulses in SiPM #1 are almost not visible in SiPM #2, whereas the 3-photon pulse becomes more visible, indicating a higher direct crosstalk probability.

C. Primary dark count rate

We performed the dark measurements and analysis described above at different bias voltages and temperatures. The primary dark count rate (DCR) as a function of excess bias is shown in Fig. 6. SiPM #2 has lower primary DCR (about a factor 2) than that of SiPM #1, being about 60±5 kcps against 100±8 kcps at 3 V and 20°C. They also show a similar temperature dependence, reducing of about a factor 2 every 10 degrees in the investigated range (being ~15±1 kcps at 3 V and 0°C and ~3.5±0.4 kcps at -20°C for SiPM #2).
These results are confirmed by measurements on other wafers of both types indicating that, despite the epi layers are nominally equal, the low-lifetime substrate seems to getters impurities from the epi itself.

D. Correlated noise

As for the primary DCR, we measured the crosstalk and afterpulsing probabilities as a function of excess bias. Fig. 7 shows the direct crosstalk probability and the sum of delayed crosstalk and afterpulsing (both "standard" and AP_{diff}), as a function of excess bias, at 20 °C.

The DeCT+AP probability is about 7 times lower, at a given excess bias (e.g., ~35±1 % for SiPM #1 vs. ~4±0.8 % for SiPM #2, at 2.1 V). Interestingly, in SiPM #2 the DeCT+AP probability does not diverge but seems quite constant. The overall delayed-event probability (DeCT+AP)

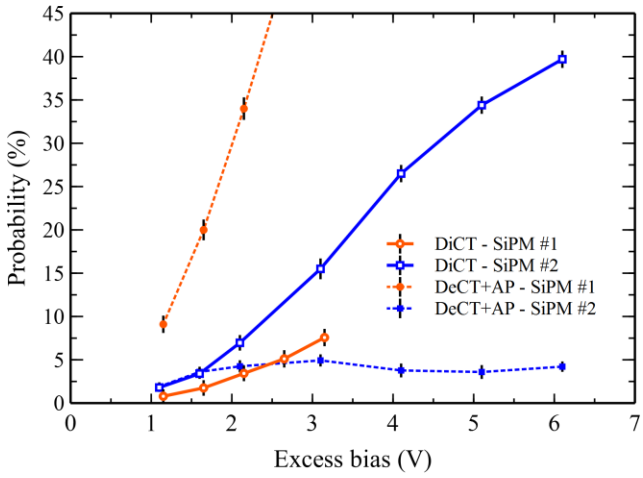

Fig. 7 Direct crosstalk probability (DiCT) and the sum of delayed crosstalk probability (DeCT) and afterpulsing probability (AP) of 1x1 mm^2 SiPM #1 and SiPM #2, as a function of excess bias, at 20 °C.

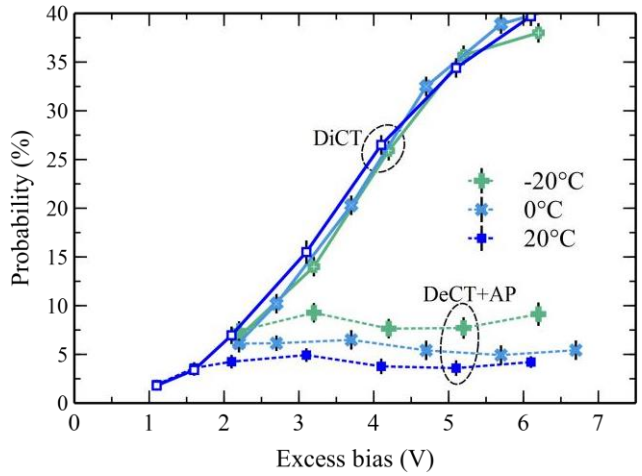

Fig. 8 Comparison of direct crosstalk probability and the sum of delayed crosstalk and afterpulsing probabilities, of SiPM #2, at three different temperatures.

for SiPM #2, at 20 °C, is always lower than 5%, also at 6 V of excess bias. The DeCT (at 20°C) gives the main contribution since the estimated afterpulsing probability increases linearly with excess bias, from zero to ~ 1% at 6 V, whereas DeCT seems to slightly fluctuate around 4 %. The reason for that behavior could be related to the depletion of the epitaxial layer at 3-4 V, as explained in the next session.

Direct crosstalk is much lower than delayed-event probability in SiPM #1, being 5±0.9 % at 2.5 V of excess bias. The opposite is happening for SiPM #2 (being DiCT ~ 10 % at 2.5 V and ~ 20 % at 3.5 V).

It is interesting to note that only in SiPM #2 the delayed component (DeCT+AP) rises with decreasing temperature. As shown in Fig. 8, it almost doubles cooling the devices from 20 °C to -20 °C, reaching about 8-10 %. Possible reasons could be the dependence of the carrier lifetime with temperature or the increment of afterpulsing probability, combined with the high DiCT probability. Further investigations are in progress to better understand this behavior.

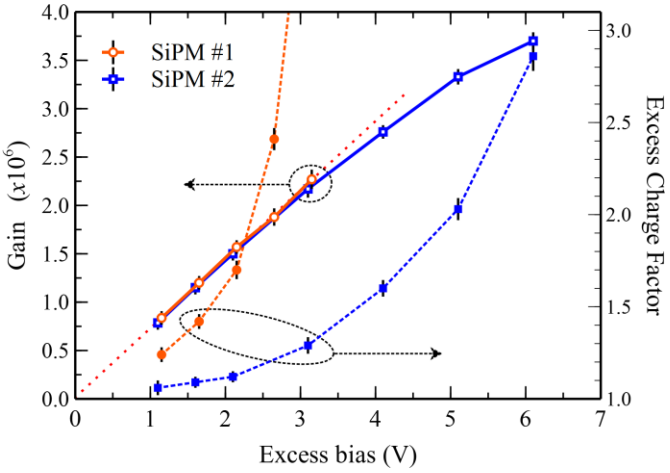

Fig. 9 Gain and excess charge factor (ECF) of SiPM #1 and SiPM #2, as a function of excess bias, at 20 °C.

Note that the distinction between DiCT and DeCT can be slightly affected by read-out system and, in particular, by the acquisition rate and bandwidth. When the events are very close (few nanosecond) the delayed crosstalk may not be distinguished from the primary pulse and thus be counted as a direct cross-talk. The sum is not altered of course. The excess charge factor, ECF (see next section), instead, is estimated from the reverse current, the gain and the primary DCR, thus it does not suffer from this uncertainly.

E. Gain and excess charge factor

As shown in Fig. 9, the gain is equivalent for SiPM #1 and #2 (since they share the same cell layout), being ~$1.5\pm0.1\cdot10^6$ at 2 V, and it is linear up to about 3-4 V. At higher biases the gain of SiPMs have a less-than-linear behavior. This is related to the depletion of the epitaxial layer: while at breakdown the depleted region is confined within the implants (as in Fig. 1), increasing the bias it extends to the bottom of the epitaxial layer. The growing depletion lowers the cell capacitance with the bias thus the gain starts growing less than linearly.

It is also interesting to quote the excess charge factor (ECF). It gives an indication of the overall SiPM correlated noise since it quantifies the amount of "extra charge" the SiPM produces per each primary generated carrier, due to AP and CT. It is calculated as the current flowing through the SiPM, at a given bias, divided by the elementary charge (q), by the primary dark count rate and by the gain. An ECF of 1 means no correlated noise. For SiPM #1 it is about 1.7±0.05 at 2.1 V of excess bias and it diverges to more than 3 at 3 V. For SiPM #2, it is much lower, being ~ 1.12±0.03 at 2.1 V and < 2 at 5 V. Therefore, even with the increase of direct cross-talk, summing the contributions to correlated noise probability, SiPM #2 has a significantly lower excess charge factor than SiPM #1.

F. Quenching resistor and recovery time

Another interesting implication of the reduced delayed-correlated events is the possible reduction of the quenching resistor (R_Q), and consequently of the recharge time. In SiPM #1 a long recovery time is needed (> 200ns) to keep the cell in a "dead" state for a longer time after an avalanche. This reduces the AP_{diff} and the positive feed-back which limits the operating bias voltage. In order to set the desired dead time we implemented a quenching resistor of about 2 MΩ. However, in some applications a long dead time is undesirable.

In case of substrate #2, the correlated noise probability is much lower so we can decrease the quenching resistor. To verify this we produced two types of devices: one with the same R_Q of SiPM #1 (shown in the plots before for direct comparison) and another with R_Q = 700 kΩ. Despite the recovery time is reduced by a factor 3 (to 70 ns) we did not observe any significant reduction of operating voltage. We only noted a little increment of the afterpulsing probability (still AP due to trapped and released carriers), of about 50 %. However, since DeCT is still dominant over AP, the increment in DeCT+AP is only 10-15%.

The R_Q value cannot be reduced much further because it would reduce the maximum operating over-voltage because of inefficient quenching [17].

G. Photon detection efficiency

We measured the photon detection efficiency as a function of wavelength and excess bias. To make the measurement less affected by correlated noise and much faster, we measured the PDE of a "single-cell SiPM". It is essentially a SPAD with integrated resistor identical to one SiPM cell, with exactly the same layout and taken from the same wafer. In the measurements, we obviously considered the fill-factor of the cell when composing the SiPM. We previously checked the consistency of the PDE measured with SiPMs of different sizes on various productions validating the results obtained from the single cell.

We used a setup composed by an integrating sphere with 3 ports. A monitoring photodiode was always placed on one port (attached to the sphere) and the SiPM under test on another port, at a distance of ~10 cm (to have good irradiation uniformity). The setup was previously calibrated using a calibrated detector (Newport 818-UV) in place of the SiPM. We measured the photocurrent from the monitor diode and the calibrated one, obtaining the irradiance ratio as a function of the wavelength. As a light source, we employed either a broadband lamp coupled to a monochromator or pulsed LEDs (commercial LEDs with different emission central wavelengths), with a typical optical FWHM of about 10 nm. The light from the monochromator or one LED was injected in the integrating sphere through an optical fiber.

First, we measured the PDE with the LEDs in pulsed mode counting the percentage of triggers from the detector out of the total light pulses. This was done for several wavelengths in the NUV and blue wavelength region (between 350 nm and 450 nm) and on few wavelengths in the green and red region. Then we scanned the light spectrum with the monochromator in continuous illumination mode, measuring the current from the detector, with and without light. Then, we normalized the plots to the data obtained from the green and blue LEDs. In all the measurements, the DCR or current in dark was subtracted.

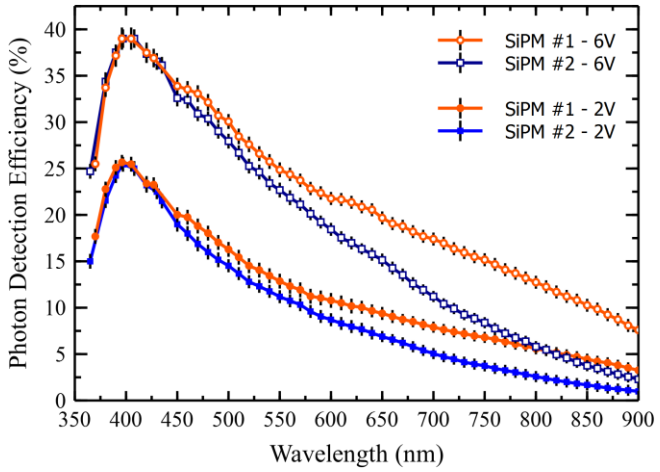

Fig. 10 Photon detection efficiency (including the fill-factor) as a function of wavelength for different excess bias, at 20 °C.

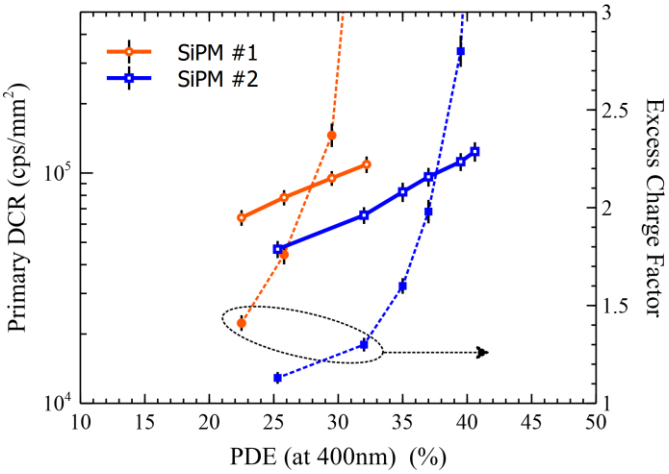

Fig. 11 Plots of primary DCR and Excess charge factor as a function of photon detection efficiency at 380 nm, for SiPM #1 and SiPM #2.

The detection efficiencies of both SiPM #1 and SiPM #2 are shown in Fig. 10, as a function of the wavelength. It can be seen that for both devices, the PDE peaks in the range 390-410 nm, reaching values higher than 25 % with 2 V of excess bias and of about 40 % at 6 V of excess bias.

At very short wavelengths (< 380nm), the epoxy resin deposited on top absorbs part of the light. This produces the fast reduction in PDE. We measured also a device without epoxy and we obtained a PDE that at 350 nm is still higher than 30%, with 6V of excess bias.

PDE of SiPM #1 and SiPM #2 have similar shapes but in SiPM #2 it gets lower at longer wavelengths, compared to SiPM #1 the PDE is ~65% at 700 nm and ~45% around 800 nm. This is a direct consequence of the lower lifetime of the substrate #2: at short wavelength all the photons are absorbed inside the depleted region, instead, at longer wavelengths, part of the photons are absorbed in the substrate and have to diffuse to the depleted region to trigger the avalanche pulse. In SiPM #1 the diffusion length is much higher than in SiPM #2, increasing the amount of photo-generated carriers collected thus the photon detection efficiency.

The PDE is the product of the quantum efficiency, i.e. the amount of photo-generated electron-hole pairs with respect to the total incoming photons in the active area, the avalanche triggering probability and the cell fill-factor. As a first approximation, in the calculation of quantum efficiency, we considered as the effective thickness (i.e. the region where photo-generated carriers can reach the active region without being re-absorbed) the sum of epi-layer thickness and half of the diffusion length of holes in the substrate. Using this approach, we estimated a ratio between PDE of SiPM #2 and #1, of ~95% at 500 nm, ~75% at 600 nm, ~60% at 700 nm and ~55% at 800 nm, which is in agreement with the measurements.

It is generally useful to plot the dark count rate and ECF as a function of detection efficiency, as shown in Fig. 11. With such a representation we can evaluate the max PDE we can reach at a certain wavelength given a certain amount of correlated noise/primary noise or vice versa. If we consider a maximum ECF of 2, we can operate the SiPM #1 at a PDE of ~27% and primary DCR of 80kcps, whereas, the SiPM #2 reaches a PDE of ~37% and a primary DCR of ~90 kcps.

H. Photon number resolving capability

Finally, we characterized the photon-number resolving capability of the SiPMs. We illuminated the devices with a pulsed LED illumination. The LED was directly connected to a fast-pulser, with adjustable pulse amplitude and duration. The measured width of optical pulses were in the order of few ns FWHM. Having the oscilloscope synchronized with the pulser, we recorded thousands of waveforms and created the histogram of the charge. We settled an integration time of 1 µs in all conditions.

The peaks are expected to follow the Poissonian statistics of incoming photons, enlarged by the crosstalk (both direct and delayed). The peak width is determined by the electronic noise and by possible cell-to-cell non-uniformity. The peak to valley ratio is an important feature (indicating the ability to distinguish the peaks) and it is typically limited by phenomena giving a fractional charge in the integration window such as afterpulsing, primary noise and delayed crosstalk.

Fig. 12 shows a first comparison between charge histogram acquired with SiPM #1 and SiPM #2, biased at 2 V and at a temperature of 20 °C. Light intensity has been regulated in each measurement to have a charge histogram peaked at 8 triggered cells. They all show a good peak separation at very low photon number, with a peak-to-valley ratio higher than 10, but the high delayed crosstalk probability in SiPM #1 causes a fast deterioration when the number of triggered cells increases, eventually making impossible to distinguish the peaks. SiPM #2, instead, has a much better photon-number-resolving performance: the peak-to-valley ratio is in the order of 50 at 8 triggered cells, and it remains very good up to 20. This is a very good result and, to characterize this aspect more in depth, we illuminated the SiPM #2 with increasing number of photons. As shown in Fig. 13, we used light pulses triggering on average 9, 18, 34 and 50 triggered cells. The peaks are clearly distinguishable in all conditions, with a peak-to-valley

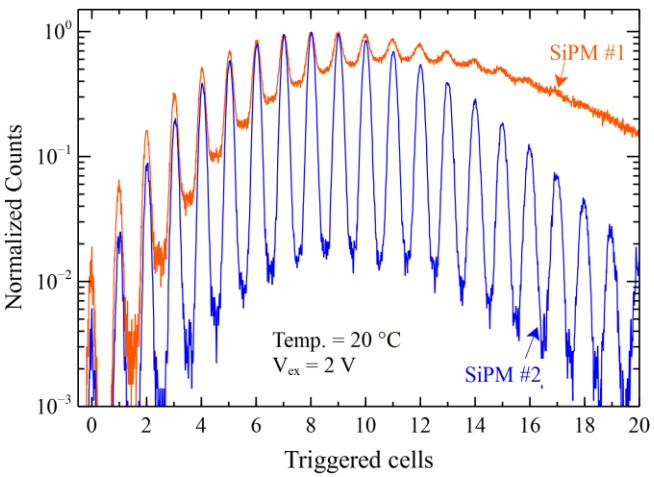

Fig. 12 Charge histogram collected with SiPM #1 and SiPM #2 biased at 2 V and at 20 °C (light intensity regulated to have the peak at 8 photons).

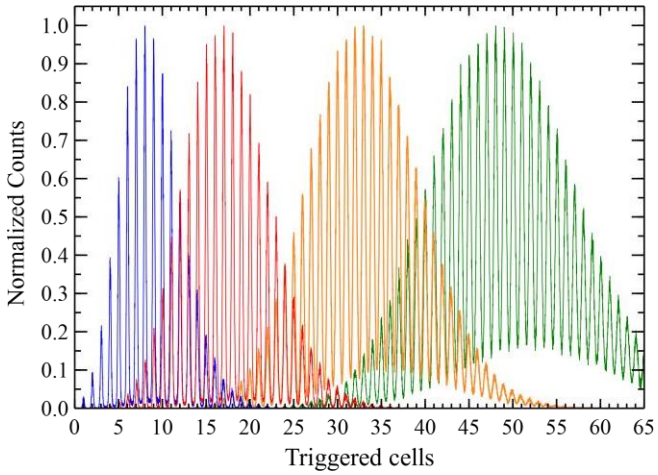

Fig. 13 Charge histogram collected with SiPM #2, at 20 °C and 2 V of excess bias, with light intensities of 9, 18, 34 and 50 average photon per pulse.

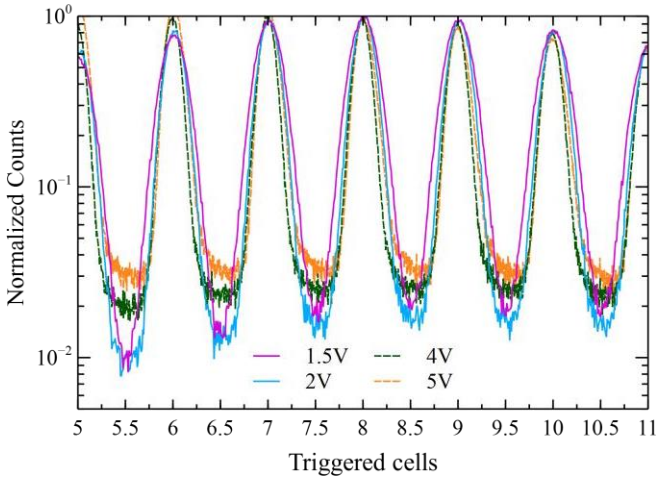

Fig. 14 Comparison of charge histograms collected with SiPM #2, at 20 °C at different excess bias, normalized in the 8-photons peak.

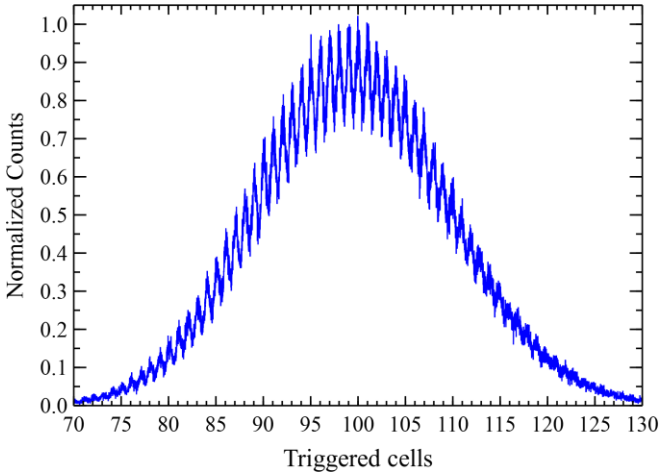

Fig. 15 Charge histogram collected with SiPM #2 (2 V of excess bias), with a high light level of 100 photons, on average, per pulse, at 20 °C.

ratio of about 7 at the higher light intensity.

This good performance of SiPM #2 does not degrade when increasing the bias: Fig. 14 shows a comparison between charge histograms at 20 °C, at different excess bias. At 1.5 V the peaks are slightly larger than in the other conditions, whereas increasing the bias the peak width reduces. At biases higher than 3-4 V, the peak-to-valley ratio slightly reduces. The degradation at low excess bias is due to the relatively small signal amplitude compared to the fixed amplitude of electronic noise. The growth of the valley level, instead, is mostly due to the increment of delayed crosstalk which increases the probability of having a fractional charge, due to delayed events generating pulses partially inside the integration window.

We finally illuminated SiPM#2 with strong light pulses, triggering ~100 cells on average. Fig. 15 shows that even at this high light intensity, the peaks are clearly visible. This is one of the best results reported in literature [16] [18] [19].

V. Conclusions

In this work, we analyzed a possible method, adding no complexity to the fabrication technology, to reduce the correlated noise in silicon photomultipliers, which is an important and unwanted noise source. We focused on afterpulsing and crosstalk components originated by carriers diffusing from the substrate. To study these noise components we produced NUV-SiPMs on two different silicon materials featuring substrate carrier lifetime differing by a factor of approximately 200 for the purpose of modulating the recombination of the carriers generated by the photons emitted during an avalanche.

This solution proved to be effective: the delayed crosstalk and the afterpulsing are strongly reduced in the substrate with lower lifetime. Now it is low enough to not limit the maximum operating excess bias for a higher detection efficiency as well as the intrinsic time resolution [7][20].

A side effect we found using this substrate is a higher direct crosstalk probability: this is an unwanted behavior, which will require further investigations to be better understood. However, summing up the contributions of the different correlated noise components, the measured excess charge factor is highly reduced. This gives the SiPM a very good photon-number resolving capabilities.

We also noticed that the SiPM made with the low-lifetime substrate features a lower primary dark count rate and also lower detection efficiency in the red wavelength region: the latter is due to the lower carrier "collection depth" in the substrate.

To further reduce the correlated noise, thus improving the SiPM performance, other actions can be undertaken: i) to reduce the cell gain (thus the number of emitted photons during the avalanche) decreasing the cell dimensions, and ii) to implement trenches between cells, creating a barrier for photons to reach neighboring cells. These further developments are similar to what we did in the RGB-HD technology [19]. These solutions also allow increasing the cell fill-factor, thus also the PDE of the SiPM.

REFERENCES

[1] D. Renker, "Geiger-mode avalanche photodiodes, history, properties and problems," Nucl. Instrum. Meth. A, vol. 567, pp. 48-56, 2006.

[2] D. W. Townsted, "Multimodality imaging of structure and function," Phys. Med. Biol., vol. 53, no. 4, pp. R1-R39, 2008.

[3] W. W. Moses, "Recent advances and future advances in time-of-flight PET," Nucl. Intrum. Meth. A, vol 580, pp. 919-924, 2007.

[4] G. Muehllehner, J. S. Karp, "Positron emission tomography." Phys. Med. Biol., vol. 51, no. 13, pp. R117-R137, 2006.

[5] S. Surti, A. Kuhn, M. E. Werner, A. E. Perkins, J. Kolthammer, J. S. Karp, "Performance of Philips Gemini TF PET/CT scanner with special consideration for its time-of-flight imaging capabilities" Journal of Nuclear Medicine, vol 48, no. 3, pp. 471-480, 2007.

[6] C. W. E. Eijk, "Radiation detector developments in medical applications: Inorganic scintillators in positron emission tomography," Radiat. Protect. Dosimetry, vol. 129, no. 1–3, pp. 13–21, 2008

[7] T. Pro, A. Ferri, A. Gola, N. Serra, A. Tarolli, N. Zorzi, C. Piemonte, "New development of Near-UV SiPMs at FBK," IEEE Trans. Nucl. Sci., vol. 60, no. 3, pp. 2247-2253, Jun. 2013.

[8] C. Jackson, k. O'Neill, L. Wall, B. McGarvey, "High-volume silicon photomultiplier production, performance, and reliability," Optical Engineering, vol. 53, no. 8, pp. 081909 1-10, Aug 2014.

[9] Ketek, "PM1150 datasheet", www.ketek.net

[10] N. Serra, A. Ferri, A. Gola, T. Pro, A. Tarolli, N. Zorzi, C. Piemonte, "Characterization of new FBK SiPM technology for visible light detection," J. Instrum, vol. 8, p. P03019, Mar. 2013

[11] C. Piemonte, "A new silicon photomultiplier structure for blue light detection," Nucl. Instrum. Meth. A, vol. 568, pp. 224–232, 2006

[12] M. Mazzillo, S. Abbisso, G. Condorelli, D. Sanfilippo, G. Valvo, B. Carbone, et. al., "Enhanced Blue-Light Sensitivity P on N Silicon Photomultipliers," IEEE Nuclear Science Symposium and Medical Imaging Conference Record, 2011, pp. 538-543.

[13] C. Piemonte, A. Ferri, A. Gola, A. Picciotto, T. Pro, N. Serra, A. Tarolli, N. Zorzi, "Development of an automatic procedure for the characterization of silicon photomultipliers," IEEE Nuclear Science Symposium and Medical Imaging Conference Record, 2012, pp. 428-432.

[14] J. Rosado, V. M. Aranda, F. Blanco, F. Arqueros, "Modeling crosstalk and afterpulsing in silicon photomultipliers," Nucl. Instrum. Meth. A, to be published, http://dx.doi.org/10.1016/j.nima.2014.11.

[15] M. Ghioni, S. Cova, A. Lacaita, G. Ripamonti, "New silicon epitaxial avalanche diode for single-photon timing at room temperature," Electron. Lett., Vol. 24, no. 24, pp. 1476-1477, nov. 1988

[16] P. Buzhan, B. Dolgoshein, A. Ilyin, V. Kaplin, S. Klemin, R. Mirzoyan, E. Popova, and M. Teshima, "The cross-talk problem in SiPMs and their use as light sensors for imaging atmospheric Cherenkov telescopes," Nucl. Instrum. Meth. A, vol. 610, no. 1, pp. 131–134, Oct. 2009.

[17] S. Cova, M. Ghioni, A. L. Lacaita, C. Samori, and F. Zappa, "Avalanche photodiodes and quenching circuits for single photon detection," *Appl. Opt.*, vol. 35, no. 12, pp. 1956–1976, Apr. 1996

[18] A. Vacheret, G.J. Barker, M. Dziewiecki, P. Guzowski, M.D. Haigh, B. Hartfiel, et. al., "Characterization and simulation of the response of Multi-Pixel Photon Counters to low light levels," Nucl. Instrum. Meth. A, vol. 656, pp. 69-83, 2011.

[19] C. Piemonte, A. Ferri, A. Gola, T. Pro, N. Serra, A. Tarolli, N. Zorzi, "Characterization of the First FBK High-Density Cell Silicon Photomultiplier Technology," IEEE Trans. Electron Devices., vol. 60, no. 8, pp. 2567-2573, Aug. 2013.

[20] F. Acerbi, A. Ferri, A. Gola, M. Cazzanelli, L. Pavesi, N. Zorzi, C. Piemonte, "Characterization of Single-Photon Time Resolution: From Single SPAD to Silicon Photomultiplier," IEEE Trans. Nucl. Sci., vol. 61, no. 5, pp. 2678-2686, Oct. 2014.